Use of regular patterns-based background oriented schlieren imaging and digital image correlation for visualization of convective airflow ⊘

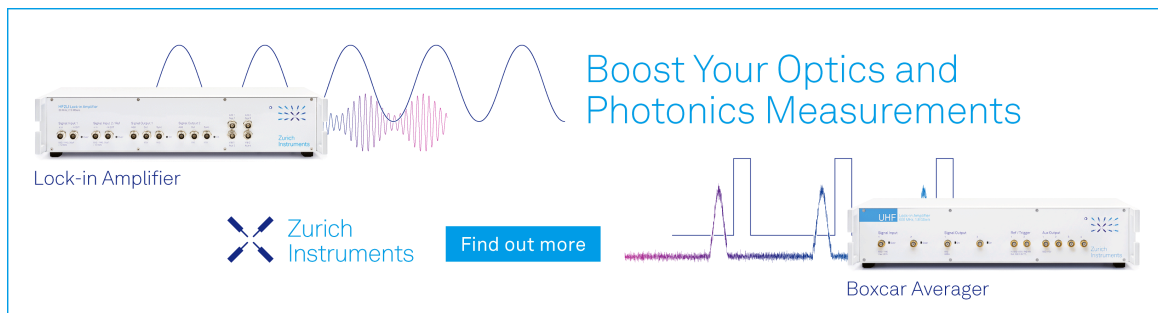Margi Sasono ✉; Setyawan P. Sakti; Johan E. Noor; Hariyadi Soetedjo

Check for updates

View Online

Export Citation

07 April 2024 23:56:24

Lock-in Amplifier

Boost Your Optics and Photonics Measurements

Zurich Instruments

Find out more

Boxcar Averager

AIP Publishing

Use of Regular Patterns-based Background Oriented Schlieren Imaging and Digital Image Correlation for Visualization of Convective Airflow

Margi Sasono[1, a)], Setyawan P. Sakti[2, b)], Johan E. Noor[2, c)] and Hariyadi Soetedjo[1, d)]

[1]*Study Program of Physics, Ahmad Dahlan University, Yogyakarta, Indonesia*
[2]*Department of Physics, Brawijaya University, Malang, Indonesia*

a)Corresponding author: margi.sasono@fisika.uad.ac.id
b)sakti@ub.ac.id
c)jnoor@ub.ac.id
d)hariyad2@yahoo.com

Abstract. Hot air rising (or convective airflow) is transparent gases (fluids) and invisible. The visualization of fluid dynamics is of considerable interest due to its widespread applications. Background-oriented schlieren (BOS) as an optical method offers numerous advantages in the visualization since this method can provide simple, non-contact, non-invasive, and non-intrusive measurements. The performance of the BOS method strongly depends on the background patterns. Implementing the BOS method usually use random dot patterns as a background and the digital image correlation (DIC) algorithm as a software tool for image processing. However, this algorithm can also analyze the regular pattern background. So far, the experimental BOS using regular patterns background and the DIC algorithm are rarely developed. In this paper, three types of regular patterns, including a checkerboard (crossed fringes), vertical and horizontal fringes patterns, have been proposed as the background in the experimental BOS. During the experiment, a camera is continuously focusing on the background patterns. At the same time, a convective airflow is in the position between the background and the camera. The digital camera records the change of background patterns with and without a convective airflow, giving them distorted and undistorted (reference) images. By comparing both images, the DIC algorithm estimates the pixel displacements. Finally, the interpolation method reconstructs the pixel displacements field into an image resembling the convective airflow. For calibration purposes, the developed BOS uses the known deflection angle of a wedge prism as a standard to assess the accuracy. As a testing, the calibrated BOS visualize the convective airflow induced by a hot object as a heat source, such as candle flame and hot plate. The results show that all the types of backgrounds in the experimental BOS has created image, visualized and distinguished the fluid dynamics of convective airflow. Also, the developed BOS can calculate quantitatively the magnitude of pixel displacements that are proportional to density (or refractive index) gradients of the convective airflow. Thus, the developed BOS can detect an invisible phenomenon and potentially measure density (or refractive index) fluids and other transparent materials.

INTRODUCTION

It is well-known that hot air rising (or convective airflow) around a heat source is transparent gases (fluids) invisible. The visualization of airflow structures (fluid dynamics) is of considerable interest due to its widespread applications from fuel injection [1], gas leakage detection [2], exhaust plumes of rocket engines [3], chemical industrial [4] to in the areas of geothermal (Earth's mantle plume) [5]. Hence, it is necessary to use a specific technique for visualizing the fluid dynamics of the convective airflow either in the laminar or turbulent flow. Optical methods offer numerous advantages in the visualization of airflow since this method can provide simple, non-contact, non-

invasive, and non-intrusive measurements [6]. Optically, the conventional way for visualizing the airflow is to record the gases refractive properties when illuminated by a beam of visible light. Since the refractive properties of gases are related to density [7], the optical method can also allow the density measurements.

One measurement technique usually used in optical methods is background-oriented schlieren (BOS). Nowadays, the BOS method has proven as a versatile tool for visualization of the various fluid media such as fluid flow [8], aerodynamics fields [9], the atmosphere [10], and shock waves [11]. Unlike the other optical method, such as the classical schlieren and shadowgraphy [12], the BOS technique is more straightforward and inexpensive in the implementation. In addition, the optical ray theory can elaborate on the principle of BOS [13]. The optical setup requires only background patterns (an imaged target), a digital still camera focused on the background patterns and suitable software for the image processing [14]. The BOS principle exploits light ray deflection angles due to the changes in the density or refractive index fluid under test integrated along the optical path [12]. An intensity changes of an image represent the light ray deflection angles captured by a camera and contain information about the density gradient (variation) of the fluid under test. The change indicator can be detected by observing distorted patterns on the background plane or extracting pixel displacements in the digital images plane. An image of BOS is finally reconstructed by digitally comparing the distorted image to an undistorted image as a reference. Thus, one of the advantages of the BOS can visualize the density gradient distribution of the fluids under test into a two-dimensional (2-D) digital image.

The BOS method can currently visualize the qualitative information and quantitative evaluation of the refractive index [7] and the density gradient in the fluid flow [14]. In principle, the BOS method relies on distorted background patterns (the imaged target) caused by the deflection of light rays from the straight-line propagation in the fluid under test [7]. The performance of the BOS measurement method strongly depends on the patterns used to mark the background. The high-resolution (high spatial frequency) and high-contrast patterns in the background are the critical factors in achieving better performance of the BOS method [15]. Thus, the design of the background plays a vital role in developing the BOS method.

Usually, developing BOS prefer to use random dot patterns as a background and common digital image correlation (DIC) algorithm as a software tool for image processing [7,16, 17,18,19]. Due to each interrogation window (sub-image) being unique, using a random dot as a background is superior in implementing the DIC algorithm to extract the pixel displacements on the BOS images. However, this DIC algorithm also can analyse regular background patterns such as checkerboard and lines or fringes [20, 21]. So far, it is rare to develop an experimental BOS using a regular patterns background and the DIC algorithm software elsewhere.

This paper proposes the regular patterns as a background and uses the DIC algorithm for analyzing and extracting the pixel displacements in the digital BOS images. The three regular (or periodic) patterns as the backgrounds are a checkerboard (crossed fringes), vertical and horizontal fringes. A convective airflow introduced by a hot object takes a position in the test section between a camera and the background. In this work, the BOS calibration process (accuracy assessment) uses the known deflection angle of a wedge prism as a standard measurement. The calibrated BOS visualize the convective airflow induced by a candle flame and hot plate as testing. An in-house MATLAB software implements the DIC algorithm to extract the pixel displacements by comparing the distorted and undistorted (reference) digital images. This work also compares the three types of regular patterns to visualize the convective airflow when utilized as a background in implementing experimental BOS.

MATERIALS AND METHODS

Technically, an optical setup of experimental BOS is simple. It requires only background patterns and a camera to capture the background images. Figure 1 shows a schematic diagram of experimental BOS. A Light Emitting Diode (LED) panel as a light source (produce white light) illuminates the background patterns, and a digital camera captures the background images. The background position is at a distance $D \gg f$ from the lens, where f is the focal length of a lens used by the camera. Thus, the background-position can be considered at infinity so that the experimental BOS can use the paraxial approximation (or parallel light rays) [7]. A hot object as a source of convective airflow takes a position in the test section between the background and the camera, and this will allow a change in the refractive index (density) caused by the different temperatures in the fluid [6] (or the air inside the test section). The parallel light rays emanating from a background patterns will experience the changes in the optical path lengths and deflect toward the area with the higher density [19]. A digital camera records the light ray deflections as a distorted background image. Technically, the focusing lens is on the background patterns, and when the focussed patterns are disturbed by the convective airflow, the sensor in the camera unit capture and record the phenomena as a distorted image.
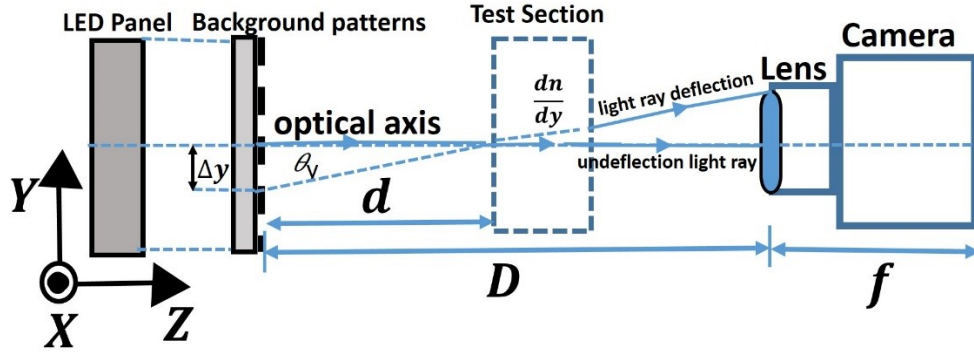
FIGURE 1. A schematic diagram of simplified experimental BOS.

According to Fermat's principle [7], the propagation of a ray through the variation of refractive index (density) is given by

$$\frac{d}{ds}\left(n\frac{d\mathbf{r}}{ds}\right) = \nabla n \tag{1}$$

where $\mathbf{r}$ is the ray position, n is the index of refraction and s is the path of rays. Using the paraxial approximation and that the ray propagates paraxially in the z-direction (Fig..1), Eq. (1) can be separated into two equations.

$$\frac{d^2x}{dz^2} = \frac{1}{n}\frac{\partial n}{\partial x} \quad \text{and} \quad \frac{d^2y}{dz^2} = \frac{1}{n}\frac{\partial n}{\partial y} \tag{2}$$

By integrating once Eq. (2) with respect to z, the deflection angles in the x and y-directions of the light ray at the position (x, y) can be obtained as [23],

$$\theta_{\mathbf{x}} = \left(\frac{dx}{dz}\right) = \frac{\Delta x}{d} = \frac{1}{n_o}\int\left(\frac{dn}{dx}\right)dz \quad \text{and} \quad \theta_{\mathbf{y}} = \left(\frac{dy}{dz}\right) = \frac{\Delta y}{d} = \frac{1}{n_o}\int\left(\frac{dn}{dy}\right)dz \tag{3}$$

where n_o is ambient refractive-index, $\left(\frac{dn}{dx}\right)$ and $\left(\frac{dn}{dy}\right)$ represent the refractive index variation (gradient) in the x-y plane. As shown in Fig.1, d is the distance between fluid flow (or object in the test section) and background. While the parameter Δx corresponds to the pattern displacement in the background plane. Once the displacement can be measured, a deflection angle proportional to the refractive index gradient can be obtained.

The first step in an experimental BOS is setting and conditioning the laboratory environment. The parameters such as temperature, light intensity, wind speed, and humidity are measured and controlled. A hot object takes a position in the test section, and the camera captures and records a distorted background image due to the fluid flow (convective airflow). The images were digitized with an 8-bit greyscale corresponding to 256 levels. In the next step, the DIC algorithm compares two images (the undistorted or reference and distorted images) to estimate pixel displacements. Theoretically, the pixel displacements in the digital image can be related to the pattern displacements in the background plane as in Eq.(3). More details on the basic theory of BOS can be found in the literature [13,19]. In the experimental BOS, the seeded particles in the test section, as usually employed in the PIV method, were not used. Thus, the pixel displacements can be used to trace the fluid flow.

In principle, each image subdivides into a small image known as an interrogation window, and its size determines the DIC algorithm sensitivity [18]. Using two-dimensional (2-D) correlation analysis of interrogation window pairs can obtain the pixel displacements field (distribution). Mathematically, this correlation function, R is defined as [23]

$$R(\Delta px, \Delta py) = \int_{-\infty}^{+\infty}\int_{-\infty}^{+\infty} I_1(x,y)I_2(x-\Delta px, y-\Delta py)\,dxdy \qquad (4)$$

where $I_1(x,y)$ is an undistorted (reference) image and $I_2(x-\Delta px, y-\Delta py)$ is a distorted image. Meanwhile, Δpx and Δpy denote the pixel displacements in the x-axis direction and y-axis direction, respectively. The computation of the Fast Fourier Transform (FFT) algorithm states that the cross-correlation of two functions as Eq.(4) is equivalent to a complex conjugate multiplication of their Fourier Transform as [25]

$$R(\Delta px, \Delta py) = FT^{-1}\{FT_1(f_x, f_y)\,FT_2^*(f_x, f_y)\} \qquad (5)$$

where $FT_1(f_x, f_y)$ and $FT_2(f_x, f_y)$ are the Fourier Transform of $I_1(x,y)$ and $I_2(x,y)$, respectively. Meanwhile $FT_2^*(f_x, f_y)$ represents the complex conjugate of $FT_2(f_x, f_y)$. The inverse Fourier Transform operator is notated as FT^{-1} and (f_x, f_y) is the frequency domain. The computation of Eq. (5) generates a cross-correlation surface (map) as a measure of the pixel displacement field. Subpixel resolution of the displacements can be achieved by fitting either Gaussian or paraboloidal [24] functions to the region that contains the maximum peak of the correlation map. More details on the principle of the DIC algorithm can be found in the literatures [23, 24]. Once the pixel displacements field can be estimated from Eq. (5) by using the DIC algorithm, the pattern displacements Δx proportional to density gradients field of the fluid flow under test can also be estimated.

EXPERIMENTAL SETUP

The process of experimental BOS is inside the darkroom of a laboratory to ensure the ideal condition. The light intensity and wind speed parameters in the darkroom are monitored and measured. Figure 2 shows a photograph of the optical setup in the laboratory. The main BOS components consist of a regular background pattern, a digital camera, and computer software to support image processing. This setup follows the reference [15] for better performance in the experimental BOS. As shown in Fig.2, the configuration places the candle flame and hot plate as a source of the convective airflow in the test section between the background and the camera. The position of the convective airflow under test is $d = 500$ mm relative to the background position. At the same time, the distance between the background and a camera lens was fixed at $D = 1500$ mm. These positions are the most critical parameter in determining BOS sensitivity, as found in the reference [15]. In this work, the z-direction (z-axis) is the optical axis. Thus, the density (or refractive index) gradient introduced by convective airflow is assumed to be constant along the z-direction.
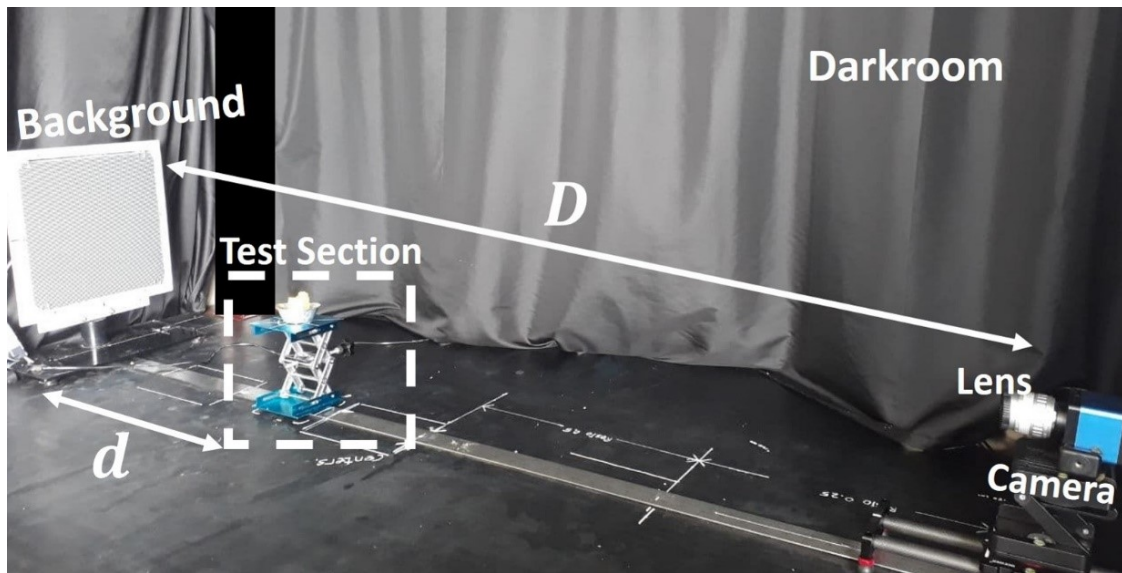

FIGURE 2. The photograph of an optical setup in developed BOS.

The first component of the developed BOS is the regular (periodic) background patterns printed on transparent materials for (30 x 30) cm as a target focused by a camera lens. The combination patterns of black-white colour are selected as a baseline to provide a high contrast background. The fringes thickness is 1 mm, and the square patterns of the checkerboard are (1 x 1) mm. A commercially available LED panel as a light source illuminates the transparent material to act as a background in the experimental BOS. In this work, three types of backgrounds with distinct variations of regular patterns are utilized, including the checkerboard, vertical and horizontal fringe patterns, respectively. In this case, all the backgrounds have a basis of sinusoidal patterns with the spatial period of 25 pixels as obtained based on the Fast Fourier Transform (FFT) spectrum. Notably, the checkerboard patterns have two orthogonal components of sinusoidal patterns.

This work uses a model Hayear as a digital camera unit. The camera specifications are 16 MP image sensor, image resolution (1800 x 1920) pixels, pixel size (1.43 x 1.43) μm, and frame speed 30 fps, respectively. A Fujian lens with a focal length of 50 mm/f1.4 acts as an imaging lens. The camera unit provides a connection to a personal computer (PC) unit for recording the video, storage, and image processing. During experiments, the focusing camera lens is on background patterns, and the camera records an undistorted background (without convective airflow) as a reference video. When the presence of the convective airflow, the camera records as a distorted video. A PC unit stores all the recorded video data. An in-house MATLAB code extracts the video data into the stacked images (frames) [25]. Conceptually, the BOS technique compares the distorted image to the undistorted (reference) image. A DIC algorithm can extract the pixel displacements based on the comparison of the digital images. Finally, the interpolating method [24] reconstructs the pixel displacements field into an image resembling the convective airflow around a hot object.

RESULTS AND DISCUSSION

BOS Calibration

The calibration process (accuracy assessment) of the developed BOS uses the known light ray deflection angles produced by a commercially available wedge prism as a standard measurement. In principle, a wedge prism introduces a uniform (constant) density (or refractive index) gradient [22]. Therefore, a wedge prism also will provide a uniform deflection angle when the light rays pass through the wedge prism area. In this work, a wedge prism of (4 x 4) cm in size was placed in the test section introducing a mean constant deflection angle of 0.57^0 (refer to the manufacturer's manual sheets). The angle acts as a standard or target of the developed BOS measurement. In principle, the calibration assesses the accuracy by comparing a standard angle and angle measured by the developed BOS. Ideally, the constant deflection angle of the light ray as a main optical property of a wedge prism will distort the background patterns and introduce a uniform pixel displacements field. This uniformity will represent the constant refractive index or density gradient at each point in the wedge prism area (or distribution).

The optical setup of the BOS calibration refers to Fig.2. The DIC algorithm extracts the pixel displacements field of the BOS images using an interrogation window of (16 x 16) pixels. Figure 3 shows the results of three types of regular pattern backgrounds. Visually, Fig.3a, Fig.3d, and Fig.3g show the raw images of checkerboard, horizontal and vertical fringes background (as captured by a camera), respectively. The pixel displacements extracted by the DIC algorithm reveal the different results for all types of backgrounds, as shown in Fig. 3 (the middle column). The small white boxes represent a selected area to zoom the pixel displacements. In this work, the arrows represent pixel displacements. As can be seen in a zoomed area, the checkerboard (Fig.3c) and horizontal fringes (Fig.3f) as a background introduces a uniform arrows distribution. As a result, the pixel displacements are also uniform or constant. In the checkerboard, the pixel displacements appear both in the x-direction and y-direction. However, the pixel displacements in the y-direction are predominant. Also, the horizontal fringe patterns (Fig.3f) introduce the pixel displacements thoroughly in the y-direction, similar to in Fig.3c (checkerboard). Due to the perpendicular direction to the horizontal fringes, the light ray deflections produced by a wedge prism strongly distorts the horizontal fringe patterns in the positive y-direction. As a result, all the pixel displacements are only uniform in the positive y-direction. Practically, there are no displacements in the x-direction. This result shows that the refractive index gradient in the wedge prism is constant and perpendicular to the light path used to illuminate the background patterns. Generally, the extracted pixel displacements in the wedge prism image are uniform, although the strength (modulus) of displacements tends to be non-uniform, as represented by the background colour in Fig.3c and Fig.3f.

In contrast, the uniform pixel displacements are not significantly appear in the vertical fringe patterns as a background, as shown in Fig.3h and a zoomed area in Fig.3i. The deflection of light rays parallel to the vertical fringe

patterns causes these results. Hence, the deflection of light rays cannot distort the vertical fringe patterns background. In other words, the vertical fringe patterns as a background in the experimental BOS cannot detect the pixel displacements of a wedge prism image. From these results, the pixel displacements extracted by the DIC algorithm follow the optical properties of a wedge prism as a calibration standard.
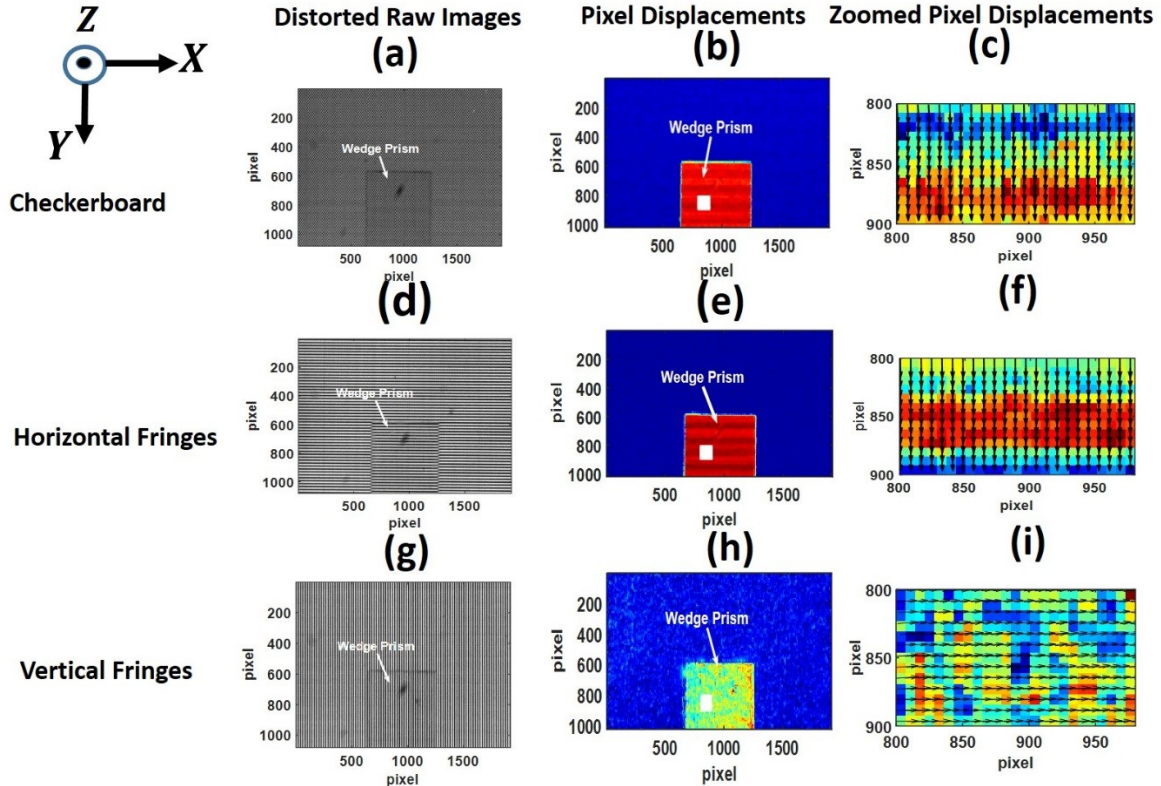
.

FIGURE 3. The image processing uses the DIC algorithm with an interrogation window of (16 x 16) pixels in the case of BOS calibration based on the known light deflection angles introduced by a wedge prism as a standard measurement. A small white box in the images is to zoom apparent pixel displacements.

The interpolation method reconstructs the pixel displacement fields into an image to visualize the distribution of deflection angles in the wedge prism. For brevity, the results show only the modulus images (scalar of the pixel displacements). The modulus images of checkerboard, horizontal, and vertical fringes backgrounds are shown in Fig.4a, Fig.4d and Fig.4g, respectively. As expected, the checkerboard image (Fig.4a) is visually similar to the horizontal fringes image (Fig,4d). Using the line profile across the image plane at horizontal line 800-row pixels (white dashed line A-B) and vertical line 1000-column pixels (white dashed line C-D), the curve of the pixel displacements relative to reference lines are more straightforward to observe. As expected, the checkerboard and horizontal fringe patterns backgrounds yield similar displacement values for all line profiles. In contrast, the background of the vertical patterns, as shown in Fig.4g, Fig.4h, and Fig.4i, cannot significantly generate the displacement curves

The displacement curves of line profile across a modulus image become the basis for calculating the mean quantitative pixel displacements as they are measured relative to the reference lines. According to Eq. (3), the mean pixel displacements are proportional to the deflection of angles introduced by a wedge prism. For brevity, this work does not present the calculations of the deflection angles as measured by the developed BOS. The calculation results show that the checkerboard and horizontal fringe patterns background in the setup as in Fig.2 yield the calculated deflection angles within less than 5% error (deviation from the standard). However, the vertical fringe patterns background cannot significantly calculate the deflection angles. Generally, the calibration results show that the developed BOS measurements have high accuracy for detecting and visualizing the deflection angle distribution corresponding to the characteristics of a wedge prism.
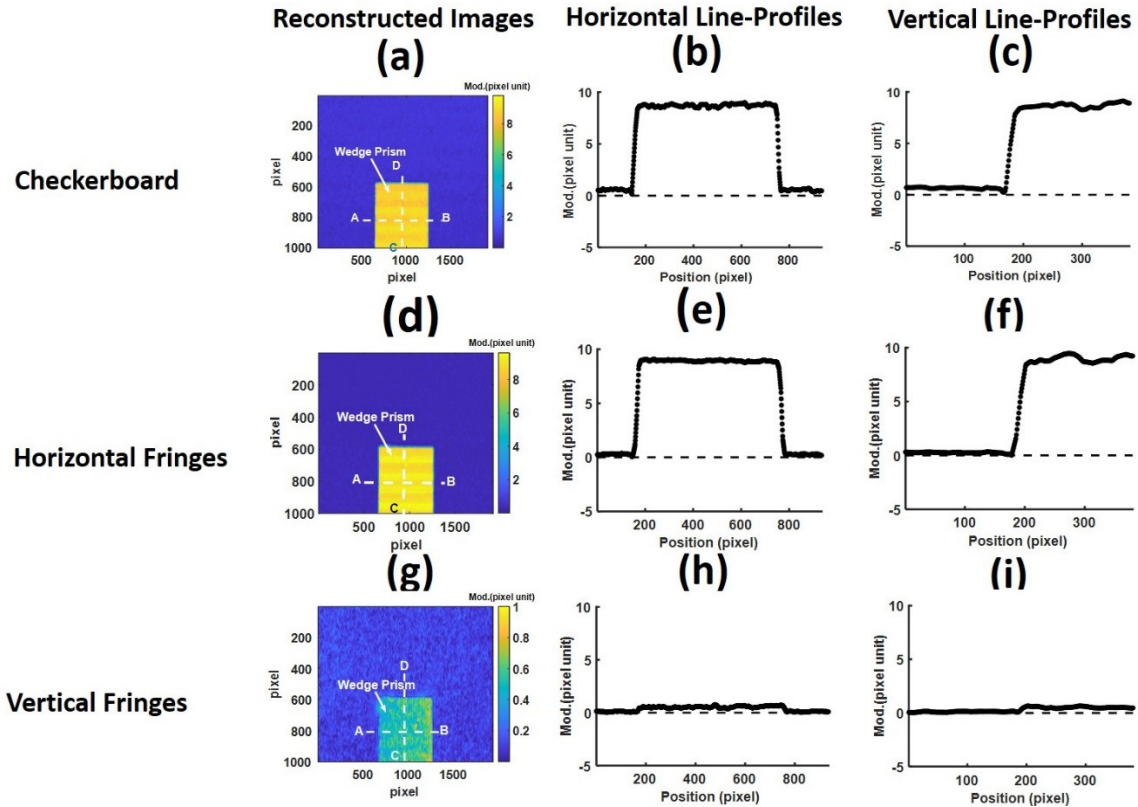
FIGURE 4. The modulus (scalar) images, horizontal and vertical line profiles across images of three types of backgrounds result from the BOS calibration process. The horizontal profile across an image is taken at position 800-row pixels (white dashed line A-B), and the vertical profile is at position 1000-column pixels (white dashed line C-D). The colorbars represent the pixel displacement values.

Test for Stable Candle Flame

The calibrated BOS visualize the convective airflow around a candle flame in stable conditions as a first test. In this condition, there is no effect of wind blow in the test section. Figure 5 shows the result of the DIC analysis using an interrogation window of (16 x 16) pixels. Visually, the appearance of the convective airflow in the distorted raw images are invisible to human eyes for all types of backgrounds, as shown in Fig.5a (checkerboard), Fig.5d (horizontal fringe patterns), and Fig.5g (vertical fringe patterns). However, the DIC algorithm can show the convective airflow through the pixel displacements field, as shown in Fig.5b (checkerboard) and Fig.5h (vertical fringes patterns), especially. Figure 5c and Fig.5i reveal the zoomed area of the pixel displacements field indicated by a small white box in Fig.5b and Fig.5h. As be seen, the results show that the obtained fields tend to be symmetrical (axisymmetrical) in the vertical direction (y-axis). The pixel displacements above the flame tip resolve into two zones. The left zone (relative to the candle flame position) is mainly toward the positive x-axis directions, and the right zone is toward the x-negative direction. Practically, there are no displacements in the y-axis direction. As a result, there is no convective airflow of a stable candle flame along the y-axis. Also, the horizontal fringe patterns as background in the experimental BOS cannot significantly reveal the pixel displacements in the case of a stable candle flame, as shown in Fig.5e and Fig.5f.

The interpolation method reconstructs the pixel displacements field resembling the convective airflow of a stable candle flame into the images as shown in Fig.6a (checkerboard), Fig.6c (horizontal fringe patterns), and Fig.6e (vertical fringe patterns). As can be seen, the checkerboard and vertical fringes background reveal a homogeneous and laminar convective airflow. The horizontal line profiles of the images taken at a position of the 600-row pixel (white dashed line) confirm these results, as shown in Fig.6b and Fig.6f, especially. However, the area above the tip flame indicates a blank zone of convective airflow. The curves of line profiles determine the pixel displacement values

proportional to the refractive index (density) gradient. Thus, the checkerboard and vertical fringes as a background can visualize the convective airflow of the stable candle flame as symmetrical and laminar with a blank zone above the flame tip. In contrast, the horizontal fringe patterns cannot visualize this phenomenon, as shown in Fig.6c (modulus image) and Fig.6d (horizontal line profile). The result confirms that due to the parallel to the horizontal fringes, the light ray deflections cannot destroy the horizontal fringe patterns background image.
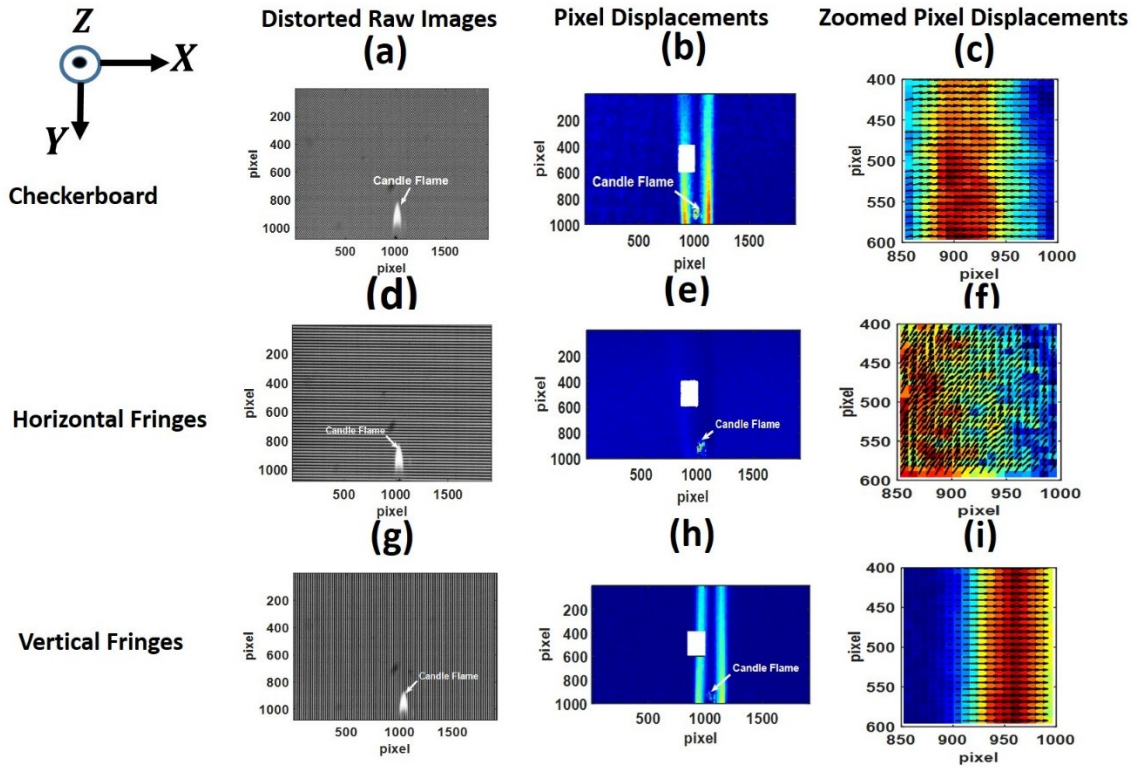

FIGURE 5. The image processing uses the DIC algorithm with an interrogation window of (16 x 16) pixels in the case of a stable candle flame. A small white box in the images zooms apparent pixel displacements.
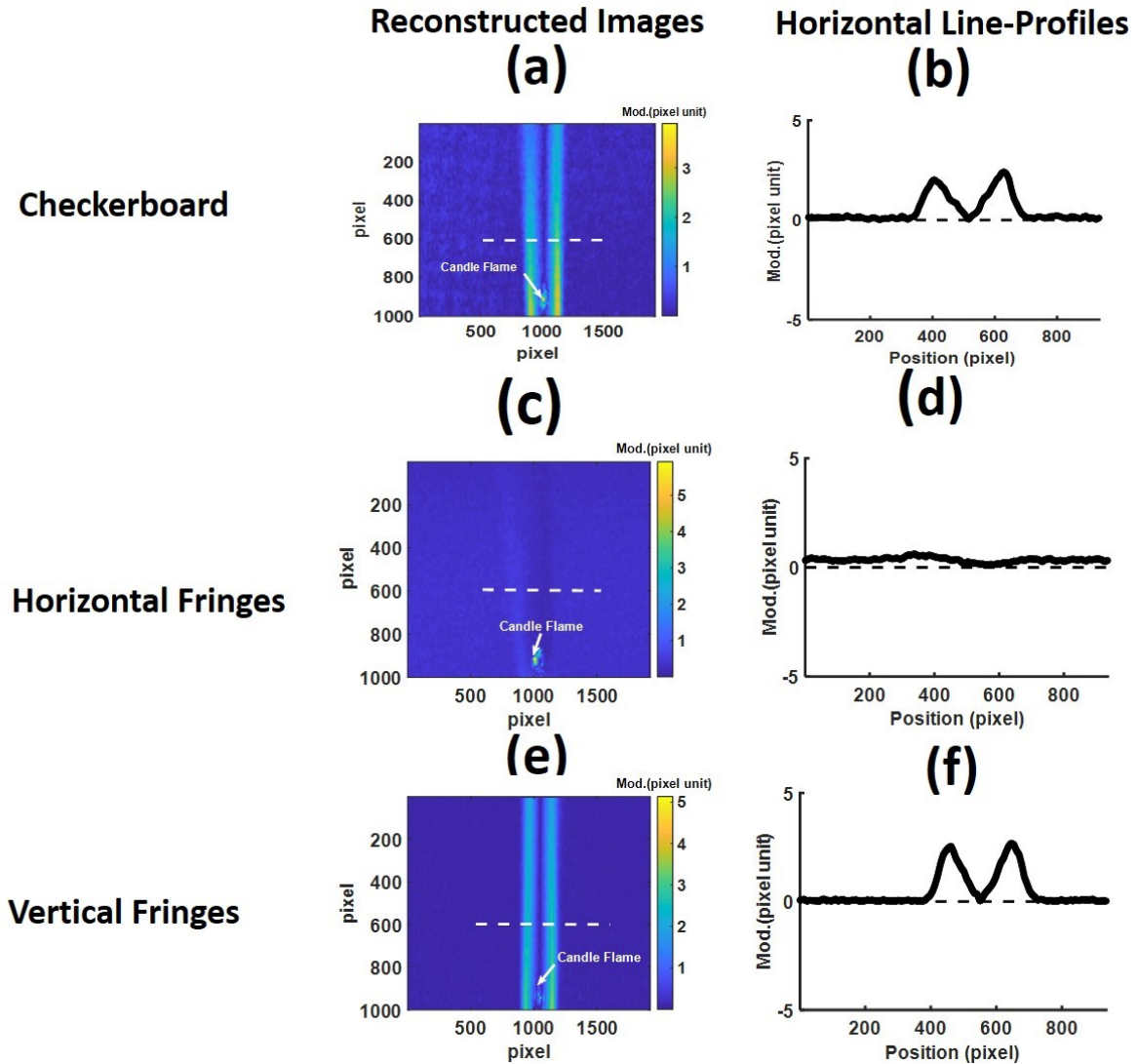
.

Reconstructed Images

(a)

Checkerboard

(b)

Horizontal Line-Profiles

(c)

Horizontal Fringes

(d)

(e)

Vertical Fringes

(f)

FIGURE 6. The modulus (scalar) images, horizontal line profiles across images of three types of backgrounds result from in the case of a stable candle flame. The horizontal profile across an image is taken at position 600-row pixels (white dashed line.). The colorbars represent the pixel displacement values.

Test for Hot Plate

In the second test, the developed BOS visualizes the convective airflow around a hot plate. The hot plate unit heats the plate until it reaches a steady temperature at 40^0 C. A digital camera captures the distorted images (raw images), as shown in Fig.7a (checkerboard), Fig.7d (horizontal fringe patterns), and Fig.7g (vertical fringe patterns). As can be seen, the convective airflow above the surface plate is visually invisible to human eyes for all types of backgrounds. However, the DIC algorithm using an interrogation window of (16 x 16) pixels can observe the appearance of the convective airflow. As shown in Fig.7b (checkerboard), Fig.7e (horizontal fringe patterns), and Fig.7h (vertical fringe patterns), the pixel displacements field (denoted by small arrows) resemble the convective airflows above the hot surface plate. The background colour represents the strength (modulus) of pixel displacements. A small white box zooms the pixel displacements field, as shown in Fig.7c (checkerboard), Fig.7f (horizontal fringe patterns), and Fig.7i (vertical fringe patterns). As can be seen, the checkerboard and vertical fringe patterns background reveal the convective airflow above the hot surface plate, as shown in Fig.7c and Fig.7i, respectively. However, the horizontal

fringe background (Fig.7f) cannot significantly reveal this physical phenomenon. Similar to the case of the stable candle flame, this result confirms that the direction of light deflections due to the density (refractive index) gradient of the convective airflow are predominantly parallel to the horizontal fringe patterns. In contrast, the vertical fringe patterns as background reveal more excellent results due to the deflection of light perpendicular to the direction of vertical fringe patterns.
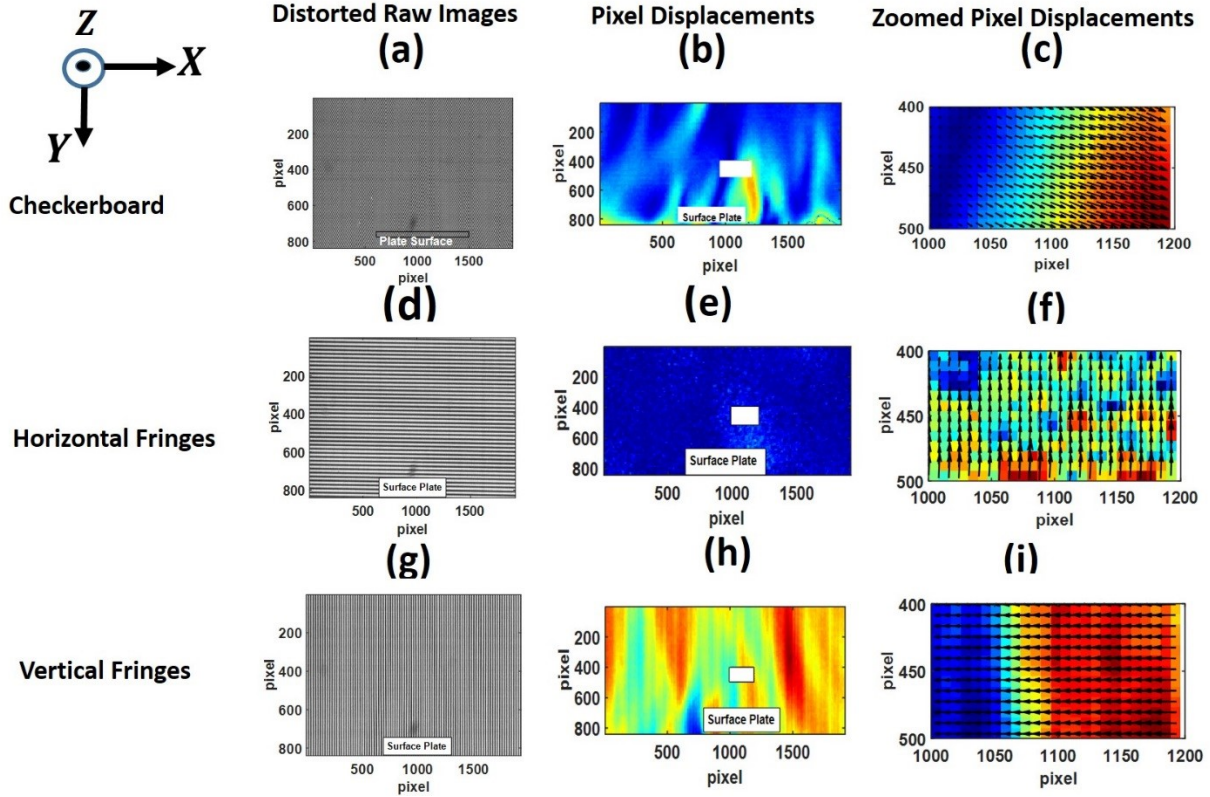

FIGURE 7. The image processing uses the DIC algorithm with an interrogation window of (16 x 16) pixels in the case of a hot plate. A small white box in the images zooms apparent pixel displacements.

.

The interpolation method can reconstruct the pixel displacements field into the modulus images resembling the convective airflows above a hot surface plate, as shown in Fig.8a (checkerboard), Fig.8c (horizontal fringe patterns), and Fig.8e (vertical fringe patterns). Visually, the convective airflows seem non-homogeneous above the hot surface plate for all types of backgrounds. Although, the horizontal fringe patterns (Fig.8c) show an insignificant result due to the light ray deflections parallel to the horizontal fringes. The horizontal line profiles taken at a position of the 600-row pixel (white dashed line) across the images confirm these results. The displacement curves reveal a variation value, as shown in Fig.8b (checkerboard) and Fig.8f (vertical fringes patterns). In contrast, the line profile of horizontal fringe patterns (Fig.8d) cannot observe the displacement curve. Despite differences in the profiles, the curves indicate the variation of the convective airflows above the surface plate. The displacement values in the curves are proportional to the light deflection angles due to the refractive index (density) gradient introduced by a hot surface plate. Unlike the checkerboard and the vertical fringe patterns, the horizontal fringes patterns as a background in the experimental BOS cannot visualize the convective airflows above a hot surface plate.
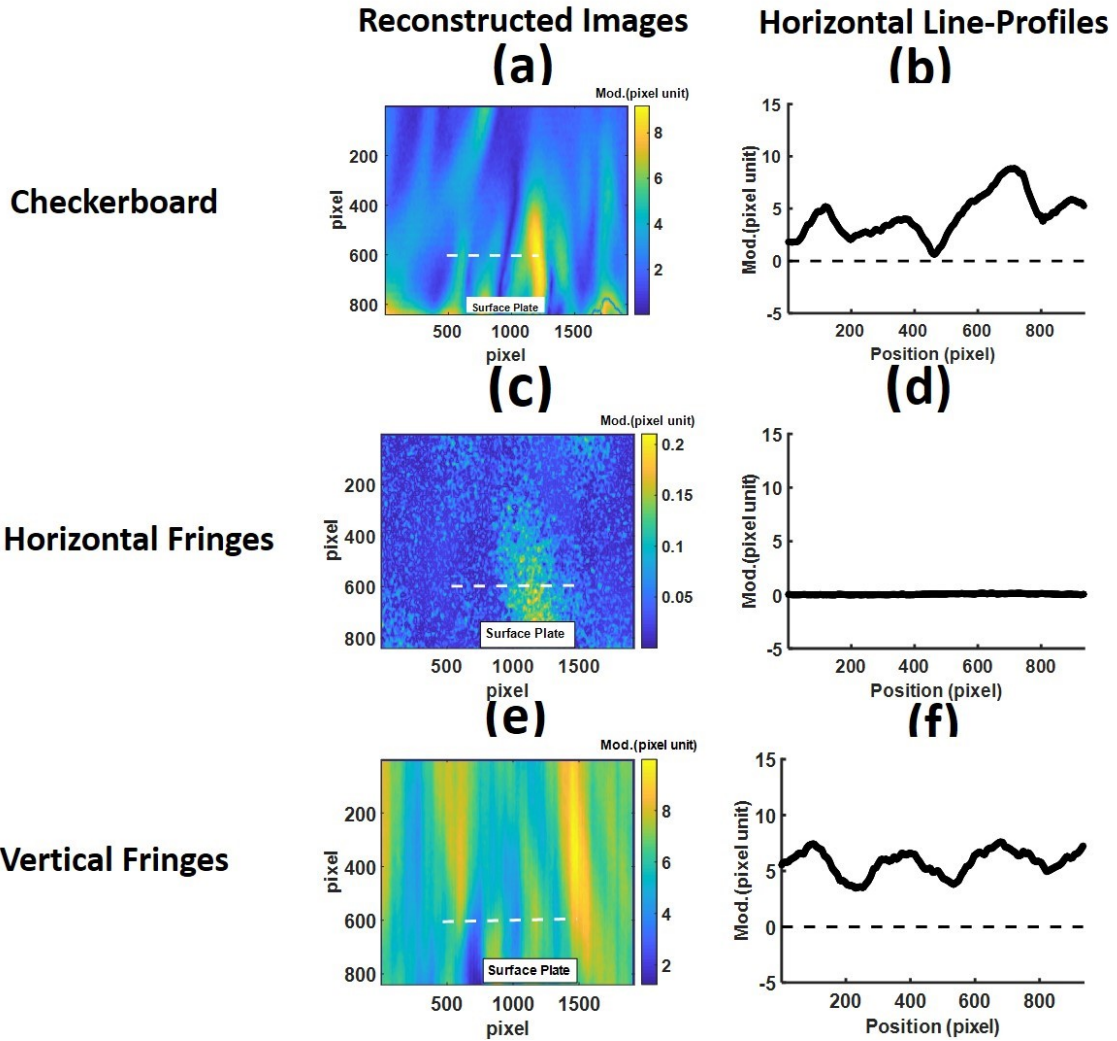
Reconstructed Images
(a)

Horizontal Line-Profiles
(b)

Checkerboard

(c)

(d)

Horizontal Fringes

(e)

(f)

Vertical Fringes

FIGURE 8. The modulus (scalar) images, horizontal line profiles across images of three types of backgrounds result from in the case of a hot plate. The horizontal profiles across an image is taken at position 600-row pixels (white dashed line.). The colorbars represent the pixel displacement values.

CONCLUSION

In this paper, the DIC algorithm based on three types of regular pattern backgrounds has been successfully developed and applied in the experimental BOS. All the background performances, including the checkerboard (crossed fringes), horizontal fringes, and vertical fringes, have been successfully tested and compared to visualize and quantify the fluid dynamics of convective airflow induced by a stable candle flame and hot plate as the hot sources. The BOS calibration (accuracy assessment) uses the known deflection angle introduced by a wedge prism as a standard measurement. The calibration results show that the checkerboard and horizontal fringes pattern were superior for measuring the deflection angle of a wedge prism within less than 5% error. However, in the case of testing for the convective airflow, the use of checkerboard and vertical fringes pattern were more feasible to obtain the image visualization of the convective airflow. Also, the experiment results show that the use of checkerboard as a background in the experimental BOS and the DIC algorithm as the tool of image processing outperforms the other regular patterns. Thus, the developed BOS can visualize qualitative (image visualization) and estimate quantitative (the pixel displacement values related to the deflection light angles due to the density or refractive index gradients) of a convective airflow. This work shows that applying the DIC algorithm based on the regular patterns has been feasible

and advantageous for further developments in the BOS technique as an optical device for measuring the distribution of density (refractive index) fluids such as gases, liquids and various other transparent materials.

ACKNOWLEDGMENTS

REFERENCES

1. Alzwayi, A.S., Paul, M.C., 2014, Transition of Free Convective Flow between Two Isothermal Vertical Plates, *International Journal of Heat and Mass Transfer, Volume 76, pp., 307-316.*
2. Ting C.C., and Chen C.C. 2013 Detection of gas leakage using microcolor schlieren technique. Measurement, 46(8), 2467–2472.
3. Phillip J., Youngblood S., Grubelich M., Saul W. V., and Hargather M. J. 2016 Development and testing of a nitrous-oxide/ethanol bi-propellant rocket engine. 52nd AIAA/SAE/ASEE Joint Propulsion Conference.
4. Ccone A., Liu J., and Zhou H., 2016, Hyperspectral chemical plume detection algorithm based on multidimensional iterative filtering decomposition, *Phil.Trans. R.Soc., A Math Phys.Eng.Sci.374, 2015.0196*.
5. McDonnell, K., Molnár, L., Harty, M., and Murphy, F. 2020 Feasibility Study of Carbon Dioxide Plume Geothermal Systems in Germany−Utilising Carbon Dioxide for Energy. Energies, 13(10), 2416.
6. Guo, G.M. and Liu H., 2017, Density and temperature reconstruction of a flame-induced distorted flow field based on background-oriented schlieren (BOS) technique. Chinese Physics B, 26(6), 064701.
7. Beermann R., Quentin L., Pösch A., Reithmeier E., and Kästner M., 2017, Background oriented schlieren measurement of the refractive index field of air induced by a hot, cylindrical measurement object. Applied Optics, 56(14), 4168.
8. Moumen, A., Grossen, J., Ndindabahizi, I., Gallant, J., & Hendrick, P. (2020). Visualization and analysis of muzzle flow fields using the Background-Oriented Schlieren technique. Journal of Visualization.
9. Mizukaki T., Borg S. E., Danehy P. M., and Murman S. M. 2014, Visualization of flow separation around an atmospheric re-entry capsule at low-subsonic Mach number using Background-Oriented Schlieren (BOS). 30th AIAA Aerodynamic Measurement Technology and Ground Testing Conference
10. Traldi, E., Boselli, M., Simoncelli, E., Stancampiano, A., Gherardi, M., Colombo, V., and Settles, G. S. 2018 Schlieren imaging: a powerful tool for atmospheric plasma diagnostic. EPJ Techniques and Instrumentation, 5(1).
11. Glazyrin F. N., Znamenskaya I. A., Mursenkova I. V., Sysoev N. N., and Jin, J. 2012, Study of shock-wave flows in the channel by schlieren and background oriented schlieren methods. Optoelectronics, Instrumentation and Data Processing, 48(3), 303 310.
12. Settles, G., S., and Hargather M., J., 2017, A review of recent development in schlieren and shadowgraph techniques, *Measurement Science and Technology, 28(4),042001*
13. Bichal, A., & Thurow, B.S., (2013), On the application of background oriented schlieren for wavefront sensing *Measurement Science and Technology, 25(1), 015001.*
14. Verso, L., and Liberzon, A. 2015 Background oriented schlieren in a density stratified fluid. Review of Scientific Instruments, 86(10), 103705.
15. Gojani, A. B., Kamishi, B., and Obayashi, S. 2013 Measurement sensitivity and resolution for background oriented schlieren during image recording. Journal of Visualization, 16(3), 201–207.
16. Rajendran LK, Bane SPM, and Vlachos PP. 2019 PIV/BOS synthetic image generation in variable density environments for error analysis and experiment design. Measurement Science and Technology 11:11–14.
17. Tokgoz S., Geisler R., van Bokhoven LJA., and Wieneke B., 2012, Temperature and velocity measurements in a fuid layer using background-oriented schlieren and PIV methods. Measure Sci Technol 23(11):115,302.
18. Thielicke W., and Stamhuis E J., 2014, PIVlab – Towards Userfriendly, Affordable and Accurate Digital Particle Image Velocimetry in MATLAB. Journal of Open Research Software, 2: e30.
19. Raffel M., 2015, Background-oriented schlieren (BOS) techniques. Experiments in Fluids, 56(3).

20. Wildeman S., 2018. Real-time quantitative Schlieren imaging by fast Fourier demodulation of a checkered backdrop. Experiments in Fluids, 59(6). Springer Nature.
21. Grediac M., Blaysat B., Sur F.. 2019 Extracting displacement and strain fields from checkerboard images with the Localized Spectrum Analysis. Experimental Mechanics, Society for Experimental Mechanics, 2019, 59 (2), pp.207-218
22. Cai H., Wang Y.L., Wainner R., Iftimia N., Gabel C., and Chung S.H., 2019. Wedge prism approach for simultaneous multichannel microscopy. Scientific Reports, 9:17795
23. Blanco A., Barrientos B., and Mares C. 2016 Performance comparison of background-oriented schlieren and fringe deflection in temperature measurement: part I. Numerical evaluation. Optical Engineering, 55(5), 054102.
24. Kaso A., 2018, Computation of the normalized cross-correlation by fast Fourier transfprm, PLOS ONE, 13(9) e0203434.
25. Gong S., Liu C., Ji Y., Zhong B., Li Y., and Dong H., 2019, Advanced Image and Video Processing Using MATLAB. Modeling and Optimization in Science and Technologies.